Natural Hazards
https://doi.org/10.1007/s11069-025-07210-6

ORIGINAL PAPER

Tectonic context of Puerto Rico and the US Virgin Islands: a review of active offshore structures as a base for tsunami modeling

Hernán Porras[1,2] · **Víctor Huérfano**[2] · **José Mescua**[3,4] · **Alberto López-Venegas**[2]

Received: 16 October 2024 / Accepted: 26 February 2025

Abstract
This study provides a detailed structural analysis of the fault systems in Puerto Rico and the surrounding region. We focus on classifying fault patterns based on seismic reflection data and estimating the earthquake magnitudes for individual fault segments. Current tectonic activity is analyzed by correlating fault structures, seismicity, and deformation patterns derived from Global Navigation Satellite System measurements, offering insight into the strain distribution of the area. We identify key seismogenic sources and evaluate their potential for generating large earthquakes, emphasizing their tsunamigenic potential. The Bunce, Bowin, Investigator Fault Systems, Mona Canyon, and other regional structures are highlighted for their significant role in the ongoing tectonic deformation. This analysis offers a comprehensive understanding of local seismic hazards. It contributes to tsunami risk assessment for Puerto Rico and the Virgin Islands, providing essential information for regional disaster preparedness and future research efforts.

Keywords Tectonic of Puerto Rico · Fault pattern · Seismicity and GNSS strain · Crustal deformation · Local tsunamigenic potential

1 Introduction

Over the last 200 years, the Caribbean Region has experienced more than 100 historical tsunamis, with notable recent events such as the 2010 Haiti earthquake of magnitude 7.0 Mw (ten Brink et al. 2020). Additionally, Puerto Rico has been impacted by significant earthquakes, including the 1867 earthquake in the Virgin Islands and the 1918 earthquake in the northwest Puerto Rico trench (Barkan and ten Brink, 2010), which generated tsunamis, indicating a high likelihood of future tsunamigenic events affecting the coasts of the island (Huerfano et al., 2005).

Due to the potential threat of tsunamis, numerous studies have been conducted to assess tsunami hazards based on instrumental and historical seismicity. Early proposals by

Víctor Huérfano, José Mescua and Alberto López-Venegas have contributed equally to this work.

Extended author information available on the last page of the article

Mercado and McCann (1998) and further research by Huérfano (2003) aimed to identify earthquake source areas with tsunamigenic potential near Puerto Rico; however, these initial studies described the main parameters of the structures based on historical records and focal mechanisms without considering the geometry of the structures nor current crustal deformation.

Incomplete knowledge about seismic sources in the region directly impacts tsunami modeling for two reasons: the run-up and inundation areas are directly related to the strike and dip of the fault (Gibbon et al. 2022), and active neoformed faults with long recurrence periods are not included in these studies.

In the last decades, many studies have been published in specific areas around the island of Puerto Rico and the Virgin Islands based on seismic reflection, seismicity, crustal deformation, and geology campaigns, contributing to a better understanding of the tectonic configuration and structural style of these areas. Our goal is to compile this information, address the discrepancies among existing models, and gain a comprehensive understanding of the tectonic setting in Puerto Rico and the Virgin Islands region. The analysis will provide a regional-scale knowledge of the shallow structure and seismotectonic context in the NE Caribbean region, which is crucial for modeling tsunami scenarios.

We update and describe structures along the NE boundary of the Caribbean-North American plate, incorporating seismic reflection, seismicity, focal mechanisms, and Global Navigation Satellite System (GNSS) data. Based on this extensive database, we analyze fault patterns and divide the structures into segments to evaluate their tsunamigenic potential.

2 Tectonic evolution of the NE Caribbean plate

The study area on the northeastern edge of the Caribbean plate around Puerto Rico and the Virgin Islands has undergone a complex tectonic history since the early Cenozoic era. The region has witnessed multiple tectonic events involving reactivation of structures and blocks rotations along vertical axes (Vogt et al. 1976; Schell and Tarr 1978; Gardner et al. 1980; Speed and Larue 1991; Masson and Scanlon 1991; Mercado and McCann 1998; Mann et al. 2005; Hippolyte et al. 2005), which have been studied extensively by Chaytor and ten Brink (2010), Laurencin et al. (2017), and others.

The tectonic evolution of the study area traces back to the Cretaceous and early Cenozoic periods when the subduction of the Farallon plate along the western coast of North and Central America created an island arc known as the proto-Greater Antilles (Ross et al., 1988). The arc volcanism became profuse in the Caribbean Arc during the Late Aptian–Albian time, including Puerto Rico (Pindell and Kennan, 2009). However, there is a general lack of arc-derived tuffs in the Proto-Caribbean passive margins until the Maastrichtian–Cenozoic. Subsequent northeastward migration of the subduction zone at the eastern boundary of the Caribbean plate led to the formation of the Greater Antilles arc (Fig. 1A; Ross et al., 1988; Pindell and Barrett, 1990). A Cretaceous to early Eocene arc assemblage, consisting of accretionary prism sediments, volcanic and intrusive rocks, and ophiolites, forms the basement of Puerto Rico (ten Brink et al. 2012). In the early Eocene (~49 m.a. ago), relative North American plate motion changed to a more oblique WSW direction due to the tectonic collision between the Caribbean plate and the non-subductable

Bahamas Bank, causing the cessation of arc volcanism (ten Brink et al., 2009; Roman et al., 2021).

During the late Eocene and Oligocene (Fig. 1B), clastic and carbonatic deposits accumulated over the arc-assemblage basement (Larue 1994) and uplift, as well as rotation around a vertical axis, affected the island (Larue 1994). The low obliquity of subduction favored the transfer of compressive stresses to the arc, which, due to its basaltic/gabbroic composition, behaved as a rigid block that transmitted contractional deformation to the backarc (ten Brink and Granja Bruña, 2009). Consequently, there was a moderate uplift in the forearc and arc of Puerto Rico (Monroe 1980; Larue, 1991, 1994; van Gestel et al.

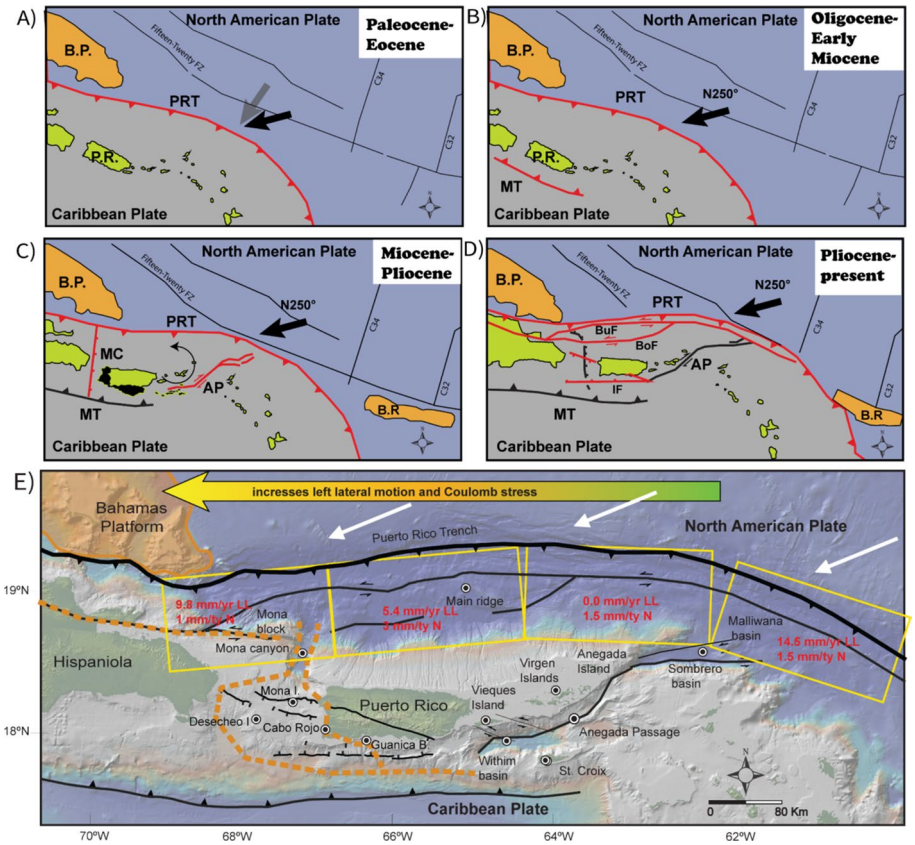

Fig. 1 Tectonic evolution based on Grindlay et al. (2005), Granja-Bruña et al. (2009), Mondziel et al. (2010), Chaytor and ten Brink (2010), ten Brink et al. (2014), Laurencin et al. (2017, 2019). Black and white arrows mean subduction convergence direction. **A** Paleocene- Early Cenozoic volcanism cessation. PRT, Puerto Rico trench. BP, Bahamas Platform. **B** Late Eocene- Early Miocene tectonic uplift. MT, Muertos Through. **C** Counterclockwise rotation. MC, Mona Canyon. **D** Forearc deformation. BoF, Bowin Fault. BuF, Bunce Fault. GPRSFZ: Great Southern Puerto Rico Fault. IF, Investigator Fault. B.R, Barracuda Ridge. **E** The different distributions of Coulomb stress due to changes in subduction slip orientation are shown in red text. Coulomb stress and motion from ten Brink and Lin (2004) is the yellow-green arrow, and ten Brink and Lopez-Venegas (2012) are represented as yellow boxes. LL, left lateral component, N, normal component. The diffuse tectonic boundary between the upper plate blocks of Hispaniola and Puerto Rico are the dashed orange lines (ten Brink et al., 2021). The main tectonic structures are shown in black lines. The white arrows represent the angle of convergence

1998). Simultaneously, a system of thin-skinned reverse faults, the Muertos retro wedge, developed in the Puerto Rico and Hispaniola backarc (Fig. 1B; ten Brink and Granja Bruña, 2009).

Subsequently, the collision of the Bahamas Platform with the Hispaniola Trench led to the counterclockwise rotation of Puerto Rico during the middle to late Miocene (Fig. 1C; Reid et al. 1991). This rotation was responsible for extensional and strike-slip faulting in the Anegada Passage (Jany et al. 1990; Gill et al., 1999; Laurencin et al. 2017). During the late Miocene to Pliocene, rifting of the Mona Canyon and strike-slip faulting in Anegada Passage potentially accommodated transtensive relative motion (Fig. 1; Jany et al. 1990; Mann et al. 2005; Laurencin et al. 2017).

By 4.5 Ma, Puerto Rico reached its current position aligned with the Caribbean plate Trench (Fig. 1C; Reid et al. 1991), and the faults in the forearc appear to represent the approximate track of the southern edge of the southeastern Bahama Province along the forearc (Grindlay et al. 2005). The movement along these strike-slip fault zones has been constrained or impeded due to the collision involving the Southeast Bahamas Province (ten Brink and Lin 2004). From this point of view, the forearc faults may represent a relatively recent addition, potentially linked to the East Septentrional Fault zone in the Hispaniola forearc (Fig. 1D). Grindlay et al. (2005) suggest a progressive process involving the subduction of a seamount, which leads to the development of scars and results in subsidence and uplift in regions such as the Mona Block and the Main Ridge (Grindlay et al. 2005).

During the Pliocene and Holocene, the Bahamas Platform is too thick and buoyant to subduct, causing it to act as a barrier, anchoring Hispaniola in place (Mann et al., 2004; Grindlay et al. 2005; Hippolyte et al. 2005; Jansma and Mattioli, 2005; Mondziel et al. 2010). As a result, Puerto Rico and the Virgin Islands gradually move eastward through extension and lateral shearing (Mann et al., 2004; Grindlay et al. 2005; Hippolyte et al. 2005; Jansma and Mattioli, 2005). The Mona Canyon, in this context, serves as an extensional zone with a fault-bounded rift characterized by vertical movements, stretching from east to west, situated between the anchored Hispaniola and the mobile Puerto Rico and the Virgin Islands (Mann et al., 2004; Grindlay et al. 2005; Hippolyte et al. 2005; Jansma y Mattioli, 2005; Mondziel et al. 2010).

At present, ten Brink and Lin (2004) suggest that the variation in strike-slip fault distance from the trench in Puerto Rico and Hispaniola results from diverse distributions of Coulomb stress due to changes in subduction slip orientation (Fig. 1E). ten Brink and Lopez-Venegas (2012) suggestt the difference in strike-slip fault distance to the trench results from resistance of the plate motion within the NE Caribbean, creating a pronounced velocity gradient (Fig. 1E). Their model indicates that the decrease in trench-parallel motion from 9.8 mm/yr in western Puerto Rico to 0 mm/yr north of the Virgin Islands, may be linked to the westward drag imparted by the Bahamas Platform (Fig. 1E). As a result, Coulomb stress decreases significantly from west to east due to the resistance of the Bahamas Platform suggesting a strain partitioning (ten Brink and Lin 2004; ten Brink and Lopez-Venegas, 2012). However, Calais et al. (2016) find that the earthquake slip vectors align with the relative plate motion in the northern sector, around Puerto Rico and the Virgin Islands (Fig. 1E). This alignment implies that the subduction occurs, with no strain partitioning.

Despite differing interpretations, both studies agree that the primary force in the forearc region is extensional. This extensional force is generated by slab retreat or

possibly a slab tear (Meighan et al. 2013) and related slab dynamics, leading to tensional stresses that promote the development of normal faults. The deformation is transferred to the backarc through the diffuse Western Puerto Rico Deformation Boundary (ten Brink et al. 2022), where the main faults Mona Canyon, Desecheo, and Investigator (described below) related to an extensional structure named Puerto Rico rifting (PR-R). However, the relationship between the forearc and backarc structures is not clear.

3 Methodology

We synthesize and refine the current understanding of Quaternary fault system geometry and kinematics of the region by compiling previously published structural maps, seismic reflection surveys, seafloor morphology, seismicity data, and GNSS data (Fig. 2). We base this analysis on the works of Grindlay et al. (2005), Granja-Bruña et al. (2009), Mondziel et al. (2010), Chaytor and ten Brink (2010), ten Brink et al. (2014), Laurencin et al. (2017, 2019) and other relevant sources as cited in the text.

3.1 Data compilation and examination

We collected and analyzed structural information from existing sources, such as structural maps and seismic reflection surveys (see Fig. 2, Grindlay et al. 2005; Granja-Bruña et al., 2009; Mondziel et al. 2010; Chaytor and ten Brink, 2010; ten Brink et al., 2014; Laurencin et al. 2017, 2019; Geist y ten Brink, 2021; Thompson-Jobe et al. 2024a, 2024b), seafloor morphology (Ryan et al., 2009) and seismicity. Seismicity data from 1982 to 2024 were acquired from the PRSN catalogs (https: www.redsismica.uprm.edu), while GPS data were sourced from Solares (2019).

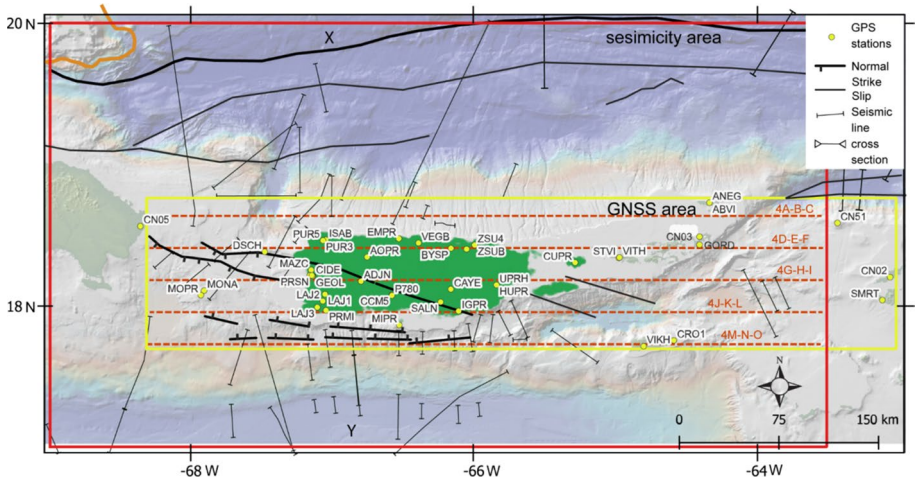

Fig. 2 **A** Compilation of interpreted seismic reflection lines; see text for references. The yellow box is the GPS interpolation area used in Figs. 4 and 5, and the red box is the seismicity area used in Fig. 3B. Red dashed lines represent the cross-sections in Fig. 4. Yellow points are GNSS stations from Solares (2019)

3.2 Segment definition and classification

Segmentation of fault structures follows the approach outlined by McCalpin et al. (2009), which involves identifying distinct fault sections using static criteria such as structural, geological, geometric evidence, and spatial discontinuities (Fig. 3A, B). These fault segments can be correlated with earthquake segments. Our subsequent categorization divided geological structures into first- and second-order faults based on their surface length and estimated depth. Both categories exhibited discernible vertical slips, observable within seismic reflection sections. Faults with a strike-slip component have been assigned a rake of −45 degrees to optimize the vertical component to evaluate the worst-case scenario that can produce bigger tsunamis. The classification of segments was then based on second-order pattern criteria. The data were compiled in QGIS to construct a structural model.

3.3 Analysis of seismicity distribution and magnitude estimation

We conducted a comprehensive analysis of seismicity distribution. This analysis examined seismic event patterns, geographical distribution, depths, magnitudes, and focal mechanisms. Relating seismicity data with the identified fault segments, we discern potential relationships between fault characteristics and seismic activity. A density map has been generated to depict the spatial distribution of earthquakes, illustrating areas with higher and lower concentrations of seismic events. Regions demonstrating elevated concentrations have been labeled seismic swarms, denoted with the prefix "S" (Fig. 3C). To estimate the seismic hazard associated with the main structures in the region, we determined the maximum possible earthquake magnitude for the faults from their surface length based on the empirical equations available in the literature (Wells and Coppersmith, 1994; Leonard, 2010). The difference between evaluations of M_w obtained by Leonard (2010) and Wells and Coppersmith (1994) is less than 5% for major faults with lengths > 10 km. The equations provided by each study are as follows:

For dip-slip faults, according to Leonard (2010):

$$M_w = 4.24 + 1.67 \log\left(L_f\right) \tag{1}$$

For strike-slip faults, according to Leonard (2010):

$$M_w = 4.17 + 1.67 \log\left(L_f\right) \tag{2}$$

And for normal faults, according to Wells and Coppersmith (1994):

$$M_w = 4.86 + 1.32 \log\left(L_f\right) \tag{3}$$

And for strike-slip faults, according to Wells and Coppersmith (1994):

$$M_w = 5.08 + 1.16 \log 10\left(L_f\right) \tag{4}$$

where L_f is the fault length in kilometers.

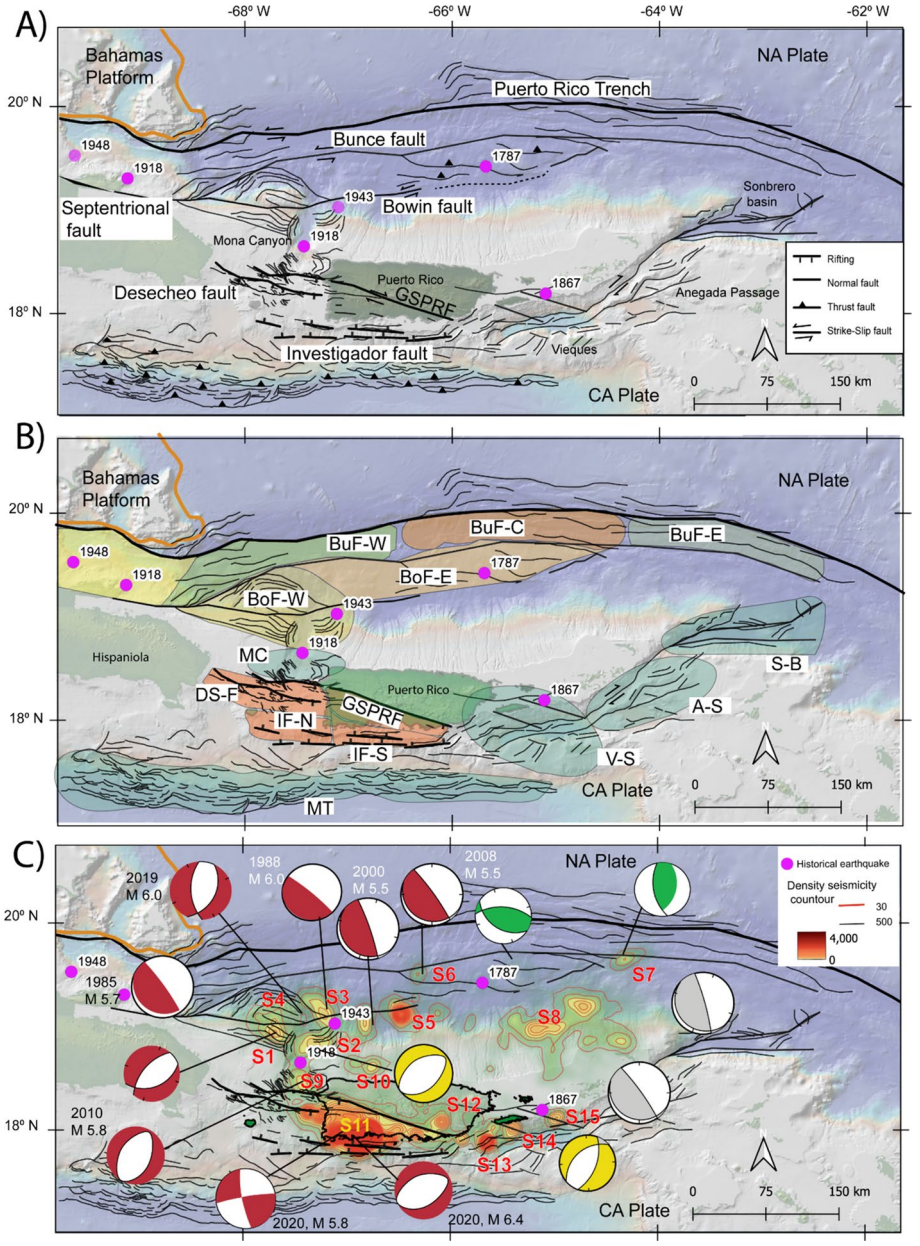

Fig. 3 **A** Tectonic map of the NE Caribbean plate (Puerto Rico) shows first and second-order structures. **B** First-order fault segmentation is based on the second-order fault pattern. BuF-E, Bunce Fault segment west; BuF-C, Bunce Fault segment central; BuF-E, Bunce Fault segment east. BoF-W, Bowin Fault segment west; BoF-E, Bowin Fault segment central. MC, Mona Canyon. DF-S, Desecheo segment; GSPRF, Great Puerto Rico Southern Fault zone. I-W, Investigator Fault segment west; I-E, Investigator Fault segment east. V-S; Vieques segment; A-S, Anegada segment; S-B, Sombrero basin; MT, Muertos Through. Colors were assigned randomly to differentiate each segment. The white arrow represents the subduction of the convergence direction. **C** Seismicity distribution density map. Seismic swarms are denoted with the prefix "S". Red focal mechanisms are from the USGS catalog, green are from Grindlay et al. (2005), yellow are 1918 and 1867 earthquakes, grey are composite mechanism from Jany et al (1990). See text for details

3.4 Strain analysis from GNSS

To evaluate the deformation dynamics, we used the displacement/velocity GNSS data and computed displacement/velocity gradient tensors and strain rates provided by Solares (2019). The quantification of internal strain, implying changes in size (dilation), rotation, and maximum shear strain in response to external forces, was modeled using the SSPX software (Cardozo and Allmendinger 2009). Vertical GNSS components were excluded from the analysis, and the strain analysis was performed in two dimensions (2D).

Employing the Grid-Distance Weighted routine, we used a grid spacing of 2 km and an alpha value ranging from 10 to 70 km. The alpha value is a constant that specifies the influence ratio of a station and decays with distance (Cardozo and Allmendinger 2009). Different alpha values delineate different observation scales, where low alpha values (e.g., $\alpha = 15$, $\alpha = 30$) produce high strain rates on a small local scale, highlighting specific areas. High alpha values (e.g., $\alpha = 50$, $\alpha = 70$) provide a broader perspective, smoothing out local peaks and showing a more general strain distribution across larger areas. Each alpha value offers a different insight into the geological dynamics of Puerto Rico, providing a comprehensive view of how strain distributes across different scales and regions.

Dilation and Maximum shear strain are dimensionless, while rotation is measured in radians. The SSPX software estimates the error as the absolute difference between the computed strain value using the displacement gradient tensor plus its error. Thus, the error is a maximum estimate (Cardozo and Allmendinger 2009), and no significative values are excluded to prevent the creation of artifacts resulting from interpolation.

3.5 Tsunamigenic potential evaluation

The tsunamigenic potential was evaluated using a comprehensive analysis incorporating fault geometry, seismicity, geological history, infinitesimal deformation from GNSS data, and regional tectonics. We use a simple but structured scoring system for evaluating each segment based on four primary criteria: potential magnitude, fault length, historical activity, and current deformation. Each criterion was assigned a score ranging from 0 to 3, reflecting the significance of the segment in each aspect. Segments that demonstrated the highest levels of risk or relevance, such as the capability to produce earthquakes of magnitude $\geq$ Mw 8, fault lengths exceeding 250 km, intense historical seismic activity, or significant deformation, were awarded three points. Segments with moderate characteristics received two points, while those with low relevance were assigned one point. If no recent or relevant activity was evident, the segment received a score of zero and could be excluded from further consideration. The total score for each segment was calculated by summing the values across all four criteria, enabling the classification and prioritization of fault segments according to their tsunami risk.

4 Results

4.1 Fault pattern based on seismic reflection analysis

4.1.1 Bunce fault system (BuF-)

The Bunce Fault is a sinistral strike-slip fault that runs parallel to the plate boundary, located only 10–20 km landward from the Puerto Rico Trench (ten Brink et al., 2004; Grindlay et al. 2005). The fault is characterized by a steep plane with an average dip of 70°, consistent with seismic reflection data (75°) and focal mechanisms solutions (60°–80°) (ten Brink, 2004; Chaytor et al., 2013; Laurencin et al. 2017). The maximum depth of the Bunce Fault is 10 km, as determined by seismic reflection, seismological data, and geometric restriction (Fig. 3A).

The Bunce Fault East Segment (BuF-E) is a narrow deformation zone that extends approximately 187 km in length. The second-order faults associate branches into several minor splays at the transition between the accretionary prism, the forearc sediment, and the basement rocks in an inherited zone of weakness (Fig. 3B; Laurencin et al. 2019). The maximum depth is 8 km, and we assigned a dip of 80°N and a maximum rake angle of − 45. The surface trace of the strike-slip and thrust system is shown by the 274°–290° trending lineaments, which vanish westward due to the large increase in convergence obliquity (Laurencin et al. 2019). The Bunce Fault Central segment (BuF-C) is characterized by a narrow deformation zone that extends approximately 244 km in length with a strike of 272°–258°. Due to its proximity to the slab, the fault plane should have a 5–10 km depth with a 70°N dip and a maximum rake angle of − 45°. This segment is characterized by a second-order fault pattern in an anastomosing system (Laurencin et al. 2019). The Bunce Fault West Segment (BuF-W) is interpreted by Martinez et al. (2002) as a strike-slip system with a mature stage of development. Mondziel et al. (2013) suggest that the BuF-W segment (Fig. 3B) is located within the unconsolidated sediments and basement and extends approximately 210 km. The 80°N dip remains constant with slight changes and does not produce significant variations in deformation along the strike, changing from N243° in the west to 274° in the east. Bathymetry data and seismic reflection sections show a horsetail fault system with several SW-NE trending oblique faults in the western termination (Rodríguez-Zurrunero et al. 2020).

4.1.2 Bowin fault system (BoF-)

The Bowin Fault (sometimes referred to as the 19° N Fault zone in some papers) is a sinistral strike-slip fault characterized by linear scarps ranging from 5 to 15 km in length. It runs parallel to the Bunce Fault and extends east of the Septentrional Fault in Hispaniola Island, connecting with the subduction zone (Grindlay et al. 2005) (Fig. 3A). This fault segment is subdivided into two segments, as shown in Fig. 3B.

Bowin Fault East Segment (BoF-E) extends approximately 230 km and lies directly south of the Main Ridge. The strike changes from 260° to 252°, and the fault displays a component of reverse dip or a transpressional character (Grindlay et al. 2005). The relief associated with the Main Ridge is attributed to an uplift due to a subducted seamount (Grindlay et al. 2005). This configuration is expected along a left-lateral shear, given the slightly oblique fault orientation relative to the GPS plate motion vector fault (Grindlay

et al. 2005). The second-order fault shows an anastomosing system in a positive flower structure with thrust faults as a predominant pattern. According to our geometric relationships, the maximum depth of the fault would be 20 km until it reaches the North American plate subducting slab under the Caribbean plate (Fig. 3B). The 1787 earthquake occurred in this segment near the Main Ridge, according to the interpretation of ten Brink et al. (2011). However, no precise records characterizing it adequately display a reverse dip or transpressional character component. Different researchers (Grinadlay et al., 2005; Mann et al. 2005; Jasma et al., 2005) have mentioned the Bowin fault (BoF-E) based on their interpretations of seismic lines. Other studies using GPS velocity data and seismicity (ten Brink and Lin 2004; ten Brink and Lopez-Venegas, 2012) suggest the segment between the Main Ridge and the Mona Canyon is inactive. Nevertheless, we will explore and discuss the hypothetical activity for tsunamigenic proposes.

Bowin Fault West Segment (BoF-W) spans 217.1 km, is 80°N-dipping with small components of oblique dip-slip motion, and strikes 276°–260° with a rake of − 45°N and a depth of 10 km. This segment has a second-order fault with normal displacements, shows a semicircular rollover pattern in the Mona Block, and is interpreted as a scar due to the subducted seamount (Grindlay et al. 2005; Mondziel et al. 2010). The rollover pattern in the Mona Block is bound by two planes; the southern plane connects directly with the Septentrional Fault, and the northern plane, which is possibly associated with a fault zone inherited from the Mona Canyon, may facilitate the internal rotation of the Mona Block (Fig. 1E).

4.1.3 Septentrional fault

The Septentrional fault west of the Mona Passage on Hispaniola Island accommodates the strike-slip component of the oblique convergence between the North American and Caribbean plates. This fault connects to the Bowinand Bunce faults in the northeastern sector (Mondziel et al. 2010), known as the Mona Block (Fig. 3B). Thissegment was developed under the influence of the Bahamas platform collision and recorded the formation of fold-thrust structures in the submarine accretionary wedge and increased turbiditic sedimentation into the Hispaniola Basin (Dillon et al. 1992).

4.1.4 Desecheo fault (DF-S)

The Desecheo Fault is a structure characterized by two principal planes with an oblique extension: Desecheo north (DF-Sn) and Desecheo south (DF-Ss), with lengths ranging from 56 to 18 km (Table 1). The fault runs between Puerto Rico and Hispaniola, from Desecheo Island to the platform in front of Punta Higuero (Fig. 3A, B). The Desecheo Fault planes have a range of strikes from 80 to 120, trending from ENE-WSW to ESE-WNW. The second-order pattern development in the Mona Passage faults are normal faults characterized by slightly inclined oblique-slip faults with a strike of ~ 131° and a dip to the south (Hippolyte et al. 2005; Thombson-Jobe et al., 2024). At the east end, these faults connect with structures recognized near Punta Higuero and Punta Guanajibo by Grindlay et al. (2005). The Desecheo Fault and related structures cut the entire thickness of the Late Oligocene-Pliocene carbonate platform sequence (Fig. 2F, Chaytor et al., 2013). The seismic activity along with this fault shows a dip-slip of normal motion (Chaytor and ten Brink, 2010; Fig. 2E). Based on the seismic section, our model represents this fault dipping to the south, with a maximum depth of 20 km.

Table 1 Fault geometry parameters

Segment	longitude centroid	Latitude centroid	Depth (Km)	Length between nodes	Width (Km)	Strike	Dip	Rake	Slip (m)
BoF-E	−65.7278	19.27928	20	117.8	21.2	260	70	−45	9.56
	−64.6689	19.51483	20	112.6	21.2	252	70	−45	9.56
BoF-W	−67.8396	19.07639	29	95.5	31.9	276	65	45	10.98
	−66.8252	19.09938	29	121.6	31.9	260	65	45	10.98
BuF-C	−65.9972	19.62226	8	105.2	8.5	258	70	−45	8.06
	−64.8419	19.70046	8	139.4	8.5	272	70	−45	8.06
BuF-E	−63.7137	19.64544	8	99.2	8.1	274	80	−45	9.2
	−62.849	19.47718	8	88	8.1	290	80	−45	9.2
BuF-W	−68.0529	19.30138	10	82.5	10.1	243	80	−45	2.02
	−67.3622	19.51875	10	72.1	10.1	261	80	−45	2.02
	−66.7571	19.55056	10	55.4	10.1	274	80	−45	2.02
DF-Sn	−67.4055	18.35196	20	29.6	20.3	101	80	−90	0.53
	−67.6708	18.37583	20	26.7	20.3	87	80	−90	0.53
	−67.8637	18.40203	20	17.8	20.3	120	80	−90	1.2
	−67.744	18.27251	20	14.2	20.3	118	80	−90	0.8
	−67.9057	18.32278	20	21.5	20.3	98	80	−90	0.8
	−67.3408	18.18667	20	11.2	20.3	84	80	−90	1.24
	−67.4806	18.20277	20	17.8	20.3	80	80	−90	1.24
	−67.6251	18.22507	20	14	20.3	108	80	−90	1.24
DF-Ss	−68.0457	18.34306	20	7.8	20.3	97	80	−90	1.85
	−68.159	18.38251	20	18.7	20.3	118	80	−90	1.85
	−68.2664	18.44892	20	10.2	20.3	134	80	−90	1.85
GSPRF-n	−66.8546	18.21377	20	30	20.3	113	80	−90	2.83
	−67.0905	18.28696	20	22.3	20.3	101	80	−90	2.83
GPRSFZ-s	−66.2451	18.00007	20	48.8	20.3	108	80	−90	0.97
	−66.5848	18.10928	20	26.8	20.3	111	80	−90	0.97

Table 1 (continued)

Segment	longitude centroid	Latitude centroid	Depth (Km)	Length between nodes	Width (Km)	Strike	Dip	Rake	Slip (m)
IF-N	−67.2329	17.86675	20	151	22	180	65	−90	2
IF-S	−66.8693	17.77493	20	180	22	180	65	−90	1.58
S-Bn	−62.5719	19.03608	20	37.4	20	236	80	−45	6.14
	−63.1393	18.90306	20	89.8	20	263	80	−45	6.14
	−63.7109	18.78776	20	33.5	20	243	80	−45	6.14
S-Bs	−63.6955	18.75804	20	44.9	20	79	80	−45	2.57
	−63.2158	18.77944	20	57.5	20	92	80	−45	2.57
	−62.7308	18.77556	20	45.4	20	88	80	−45	2.57
V-S	−65.0151	18.11045	20	51.5	20	180	80	290	2.57
A-S	−65.4001	18.00545	20	51.5	20	180	80	290	1.82
MC	−67.3844	18.74635	20	57	20	0	45	−90	2

4.1.5 Great southern Puerto Rico fault (GSPRF)

The Great Southern Puerto Rico Fault Zone is a thrust zone accompanying lateral movement (Fig. 3A, Glover, 1971; Erickson et al., 1990). The strike is 111° to 101°, and the length is ~ 140 km (see Table 1). These faults are covered by little deformed Neogene sediments (Graja-Bruña et al., 2015). The youngest rocks known to be affected by the west segment of the GSPRF (known as the Cerro Goden Fault) are Eocene in age. However, the absence of post-Eocene rocks near the fault leaves the possibility that the fault may still be active (Hippolyte et al. 2005). Mann et al. (2005) identified right-lateral strike-slip faults disrupting Holocene layers along the projected fault zone trend, suggesting recent activity. This activity is particularly evident at the western end of the fault, often referred to in publications as the Cerro Goden Fault. Offshore bathymetric and seismic reflection studies indicate the presence of a fault disrupting Holocene sediments from the coast westward into the Mona Passage (Grindlay et al. 2005; Hippolyte et al. 2005).

4.1.6 Investigator fault (IF-)

An east–west trending band of active extensional deformation along the southern slope of Puerto Rico characterizes the Investigator Fault Zone. The upper insular slope in the south of Puerto Rico shows variable longitude and a steep shelf slope related to the Investigator Fault Zone and the Jaguey spur (Case and Holcombe, 1984; LaForge and McCann, 2005). The second-order fault pattern associated with the Investigator Fault (Fig. 3A) consists of active extensional deformation. It shows differential surface expression caused by along-strike changes in the magnitude and distribution of the deformation (Granja-Bruña et al., 2009). Related to this extensional deformation, Thompson-Jobe et al. (2024a, b) describe a series of structures in southwestern Puerto Rico, including the Parguera, Lajas, Salinas faults, and Yuma and Cabo Rojo Rift. These faults show evidence of activity, including offset alluvial surfaces and submerged reefs (Thompson-Jobe et al., 2024a). It can be divided along the strike into western and eastern sectors (Fig. 3C, Table 1), separated by relay ramps.

North Investigator segment (IF-N) exhibits a pattern of deformation and seismic activity concentrated in a single major fault. Seismic data indicate that the north Investigator segment in its northern sector has an EW-trending length of ~ 151 km and dips 65°N (Granja-Bruña et al., 2015). Although the second fault pattern is E-W and NW–SE (Thompson-Jobe; 2004a, b), the focal mechanism (see Sect. 5) suggests an NW–SE fault plane similar to the pattern in the Desecheo Fault (Fig. 3B). The ridge on the north side of the Investigator Fault is a bathymetric high, suggesting a steep dip on its northern flank.

The Southern Investigator segment (IF-S) displays an east–west-trending fault composed of three individual north-dipping faults; however, it lacks seismic activity (Fig. 3B). This segment comprises three distinct faults that measure 180 km in total length. Granja-Bruña et al. (2015) characterize this fault as normal with a dip of 65°N. The southern Investigator segment has diffused surface expression with multiple minor faults contributing to a complex deformation pattern. This segment has also exhibited Holocene ruptures and the recent uplift of beach ridges, where some faults cross the shoreline, suggesting recent activity (Garrison, 1969; Mann et al. 2005).

4.1.7 Mona canyon

The Mona Canyon (MC) is a rift fault system that strikes approximately N-S and extends for about 20 km (Fig. 3B), separating the northern segments on the forearc and the southern segments on the backarc. Hippolyte et al. (2005) associated the second-order normal faults with structures trending N-S that limit the central-south sector of the Mona Canyon segment (Fig. 3B). The seismicity in the Mona Canyon segment is diffuse, and the earthquakes do not show significant depth, defining the fault pattern as a surface damage zone. In our structural model, it is represented with a listric geometry, dipping 45°–25°, with a strike of 190° following Mondziel et al. (2010). At the southern end, the Mona Canyon appears to end abruptly and is cut by the active Desecheo fault (Chaytor and ten Brink, 2010).

4.1.8 Anegada passage system

The Anegada Passage system is a significant crustal boundary between the Lesser and Greater Antilles Island arcs, consisting of a NE-SW trending broad deformation zone due to a combination of extensional and strike-slip faulting activity (Jany et al. 1990). Offshore structural changes show an increasingly oblique transtension northward along the Anegada Passage. Seismicity is scarce and is located southwest of the Virgin Islands (Laurencin et al. 2017). The Anegada Passage system is subdivided into three main segments, namely the Sombrero (S-B), Virgin Islands- Anegada (A-S), and Vieques—Virgin Islands (V-S) segments (Table 1).

The Sombrero segment (S-B) includes the Sombrero and Malliwana Basins (Fig. 1E), which are separate basins bounded by NE-SW scarps, normal faults, and E-W strike-slip transtensional faults (Laurencin et al. 2017). The Sombrero segment is a basin bordered by E-W trending echelon transtensional faults and NE-SW scarps (Laurencin et al. 2017). Anguilla transtensional faults bound the S-shaped Malliwana Basin to the south and extend west to the Sombrero Basin. The pull-apart basin system, as defined by Laurencin et al. (2017), consists of N-S to NW–SE extension and E-W to NE-SW striking second-order normal faulting structures.

The Virgin Islands-Anegada (A-S) segment is defined by strike-slip faults, which range from dextral, as described by Jany et al. (1990), to sinistral, as indicated by Raussen et al. (2013), with orientations ranging from 80° to 100°(Fig. 3B). These structures show NW–SE to N-S orientations associated with positive flower structures and elongated basins, with the main axis trending in the E-W direction (Jany et al. 1990).

Vieques—Virgin Islands (V-S) faults have sinistral or dextral displacement observed in an E-W and NW–SE direction (Laurencin et al. 2019). Normal faults characterize the pattern in strikes 45° and 135° (Holcombe, 1978; Jany et al. 1990; Raussen et al. 2013). The normal faults are more prominent and developed than the strike-slip pattern in the east sector. Based on the current seismicity, the strike-slip pattern corresponds to the most recent tectonic event.

4.1.9 Muertos through (MT)

The Muertos Trough is the southern boundary of the Puerto Rico and Hispaniola microplates (Byrne et al., 1985), is an east–west trending depression slightly concave to the

north, formed by an east–west deformed belt or an accretionary prism (Matthews and Holcombe 1974; Case and Holcombe, 1984; Jany, 1990; ten Brink and Granja-Bruña, 2009). The structure is characterized by reverse faults arranged in a sequence of elongated and subparallel ridges.

Different interpretations exist regarding the nature of this zone, with some proposing it as an accretionary wedge, while others, based on thrusting angles, argue for retro-arc thrusting rather than full-blown subduction (Byrne et al., 1985; Granja Bruña et al. 2009; Ten Brink et al., 2009). A small anomaly detected at approximately 100 km depth in tomographic results indicates potential under-thrusting, suggesting that it might be sufficient to be classified as subduction (van Benthem et al. 2013). According to this model, the Wadati-Benioff zone under Puerto Rico is interpreted as a north-dipping zone extending from the Muertos Trough to a depth of 100 km (van Benthem et al. 2013). The Global Positioning System (GPS) measurements indicate negligible relative plate motion (~ 1 mm/yr) between Puerto Rico and the Caribbean plate (Jansma et al., 2000).

The Fault geometry parameters are summarized in Table 1.

4.2 Correlating seismogenic sources with fault patterns

Shallow seismic activity in Puerto Rico is notably concentrated in specific areas, including the Mona Canyon, the zone between the Puerto Rican Trench and the Bowin Fault, the Sombrero Fault zone, and regions across southern Puerto Rico (Huérfano et al. 2005). Seismic events occurring at depths shallower than 25 km tend to concentrate along geologic structures expressed at the surface—such as lineaments, scarps, and uplifted mountains (Huérfano et al. 2005).

The seismic events in the western segment of the Bowin Fault (BoF-W, Mona block), swarms labeled S1, S2, S3, and S4, are linked to the 1943 earthquake in North Mona Passage. Their occurrences are proximal to the interactions among the Bowin, Bunce, and Septentrional Faults, where focal mechanisms show a normal sense of movement and are consistent with slip azimuths related to the 1943 earthquake (Dolan and Wald 1998; Doser et al. 2005).

In the northern part of Puerto Rico, there are small clusters of earthquakes (S5, S6) occurring along the Bowin Fault East (BoF-E) and corresponding to the Main Ridge seismic activity (Fig. 3C). The focal mechanism of this swarm indicates a reverse faulting mechanism consistent with the uplift of the seafloor (Fig. 3C, Grindlay, et al. 2005). Another swarm, S7, marks the junction between the Bowin and Bunce faults, and its focal mechanisms also display reverse faulting (Grindlay et al. 2005).

Between the Virgin Islands and the Bowin Fault, there is a cluster of seismicity (S8) with magnitudes below Mw 4 (Fig. 3C). A slab tear has been described by Meighan et al. (2013); however, it is not possible to discern fault patterns or surface features.

The Mona Canyon (MC) experiences minor earthquakes with a normal slip perpendicular to the trench (S9). The 1918 Central Mona Passage earthquake is related to this segment. The seismic swarm observed in S10 shows a normal mechanism. However, due to the lack of surface structures, it is not possible to associate with the BoF-W or Mona Canyon segments.

The seismicity along the Desecheo Fault is limited, mainly concentrated towards the eastern end near the GSPRF. The seismicity and strain patterns in southwestern Puerto Rico are characterized by two sets of events, one associated with a shallower extensional NW–SE regime and the other responding to the oblique contraction of major plates in

North America and the Caribbean (see Fig. 2B; Huérfano et al. 2005). While no historical evidence exists of major earthquakes in the southwestern Puerto Rico seismic zone, moderate seismic activity is considered normal. However, in the Lajas Valley, faults with surface expression faults excavated by Prentice and Mann (2005) and detected using LiDAR imagery by Thompson-Jobe et al. (2024a) indicate occurrences of significant earthquakes in the area.

The concentration of seismicity in the area is mainly south of the GSPRF and at depths < 30 km (Huérfano et al. 2005). A notable observation is the distribution of shallow epicenters around prominent topographic features and linear belts of serpentinites, particularly in Sierra Bermeja, where hypocenters at depths of 5–15 km exhibit concentration in an east–west plane with an inclination of approximately 45° (Huérfano et al. 2005). Intermediate earthquakes (25–50 km) are situated offshore, south of the Lajas Valley and southwest of Mayagüez, with events southwest of Mayagüez displaying a distinct NE-SW vertical distribution (Huérfano et al. 2005).

The eastern segment of the Investigator Fault (S11) shows seismic activity and focal mechanisms characterized by extensional and strike-slip faults. The focal mechanism suggests that the Investigator Fault (IF-) is undergoing extension, and its movement is characterized by stretching, consistent with the overall tectonic activity in that area. The second-order fault pattern is linked to the Mw 6.4 Guánica earthquake (S11, seismic swarm) on January 7, 2020, at a depth of 10 km (ten Brink et al. 2022) and is aligned with the subsidence observed in Guánica Bay. This extensional displacement is also evident in seismic lines (Granja-Bruña et al., 2016). In the southeastern region, the Anegada Passage in the Vieques-Virgin Islands segment displays limited seismic activity. Most earthquakes are northwest of the Virgin Islands forearc and south of Barbuda Island (Laurencin et al. 2017).

The seismic events associated with the Whiting, Vieques, and Virgin Islands basins typically show depths ranging from 1 to 10 km. This seismic swarm, marked as S12, has been poorly studied, and its characteristics must be better known. Swarms S13, S14, and S15 correspond to the V-S segment, and these swarms are aligned with the trace of the normal fault with strike N45. Reflection seismic data and focal mechanisms (Jani et al., 1990) show strike-slip kinematics with a normal component for these structures. Large earthquakes can occur within this segment, as demonstrated by the seismic event in 1867 with Mw 7.3 (Chaytor and ten Brink, 2010). Therefore, the Anegada segment, where few earthquakes have occurred historically, may represent a seismic gap (Fig. 3C).

4.3 Estimation of maximum earthquake magnitude

The subduction interface south of the Puerto Rico Trench was modeled as characteristic Mw-7.9 ruptures with 190-year recurrence times, corresponding to approximately 20 percent of seismic coupling for a GPS-determined slip rate of about 17 mm/yr between North America and PRVI (Jansma et al., 2000). Interface earthquakes on the Hispaniola segment are modeled as Mw-8.0 ruptures with 200-year recurrence times, corresponding to approximately 80 percent of seismic coupling. Historically, the 1943 Mw-7.6–7.8 northern Mona Passage earthquake and the 1946 Mw-7.8–8.0 northeastern Hispaniola earthquake ruptured the Puerto Rico and Hispaniola subduction segments, respectively (Dolan and Wald 1998), and the great earthquake of 1787 Mw 8.0–8.2 probably ruptured the Puerto Rico subduction segment (McCann 1985). The up-dip and downdip rupture edges are modeled to correspond to plate-top depths of 10 and 40 km, respectively.

Table 2 Fault magnitudes derived from fault length using Leonard (2010) and Wells and Coppersmith (1994)

Segment	Total length (km)	Leonard (2010)	Wells and Coppersmith (1994)
BoF-E	230	8.12	7.94
BoF-W	217	8.07	7.9
BuF-C	244	8.16	7.97
BuF-E	187	7.96	7.82
BuF-W	210	8.05	7.89
DF-n	115.4	7.68	7.54
DF-s	71.4	7.34	7.27
IF-N	103	7.6	7.48
IF-S	60.1	7.21	7.17
SB-n	160.7	7.92	7.73
Sb-s	147.8	7.86	7.68
V–n	51.5	7.1	7.08
V-s	51.5	7.1	7.08

The development of structures in the forearc, including the Septentrional-Bunce-Bowin faults, holds the potential for earthquakes of magnitude 7 or higher (Table 2), as indicated by historical and instrumental data (Muller et al., 2010). Mueller et al. (2010) estimate the recurrence time of the Bowin Fault zone at 3900 years, projecting a maximum magnitude of Mw 7.6 using the relationships defined by Wells and Coppersmith (1994). A paleo liquefaction study attributed the liquefaction characteristics along the Manati River in northwest Puerto Rico to a very large (M ~ 7.8) earthquake possibly produced by the Bowin Fault zone about 2.4–3.2 ka (thousand years ago), suggesting a recurrence time for large earthquakes of at least 2.4 ka for the fault zone (Tuttle et al. 2023).

The estimations of maximum magnitude for each segment indicate that faults with lengths higher than 50 km can produce earthquakes with Mw 7 or higher. These faults correspond to the western, central, and eastern segments of the Bunce Fault (BuF-W, BuF-C, BuF-E), the central and west segments of the Bowin Fault (BoF-W, BoF-E), the Investigator Fault (IF-N and IF-S), the Sombrero Fault (Sb-n, Sb-s), and Vieques (V-Sn, V-Ss).

4.4 Correlating GNSS infinitesimal deformation with fault patterns

Deformation is the process that describes changes in the shape, size, or position of a region due to the action of external forces. In a two-dimensional (2D) context, the dilation rate refers to the relative change in areas within a plane, indicating whether the crust is experiencing thinning or thickening (Allmendinger et al. 2007). On the other hand, the rotation rate is defined by Allmendinger et al. (2007) as the antisymmetric part of the velocity gradient tensor and represents rotation about the vertical axis. Following geological conventions, this rotation is positive in the clockwise (CW) direction and negative in the counterclockwise (CCW) direction (Cardozo and Allmendinger 2009). In the case of shear strain, the vertical axis is generally assumed to remain fixed in 2D analysis, and the deformation manifests laterally to the right or left on a map, generating changes in shape without necessarily modifying the total area or volume (Allmendinger et al. 2007). For the dataset, we have modeled using two frames of reference (ITRF and CA) and obtained the same results,

confirming that the frame of reference does not influence the parameters we are modeling, as stated by Cardozo and Allmendinger (2009) and Allmendinger et al. (2012).

4.4.1 Dilation

For low alpha values ($\alpha = 15$, $\alpha = 30$), the points are notably dispersed and concentrated in specific areas along the longitude axis, helping to identify zones of extension or contraction. Mona Canyon (MC) and the Puerto Rico rifting (PR-R) exhibit extended positive dilation across the entire alpha range, indicating significant extensional deformation

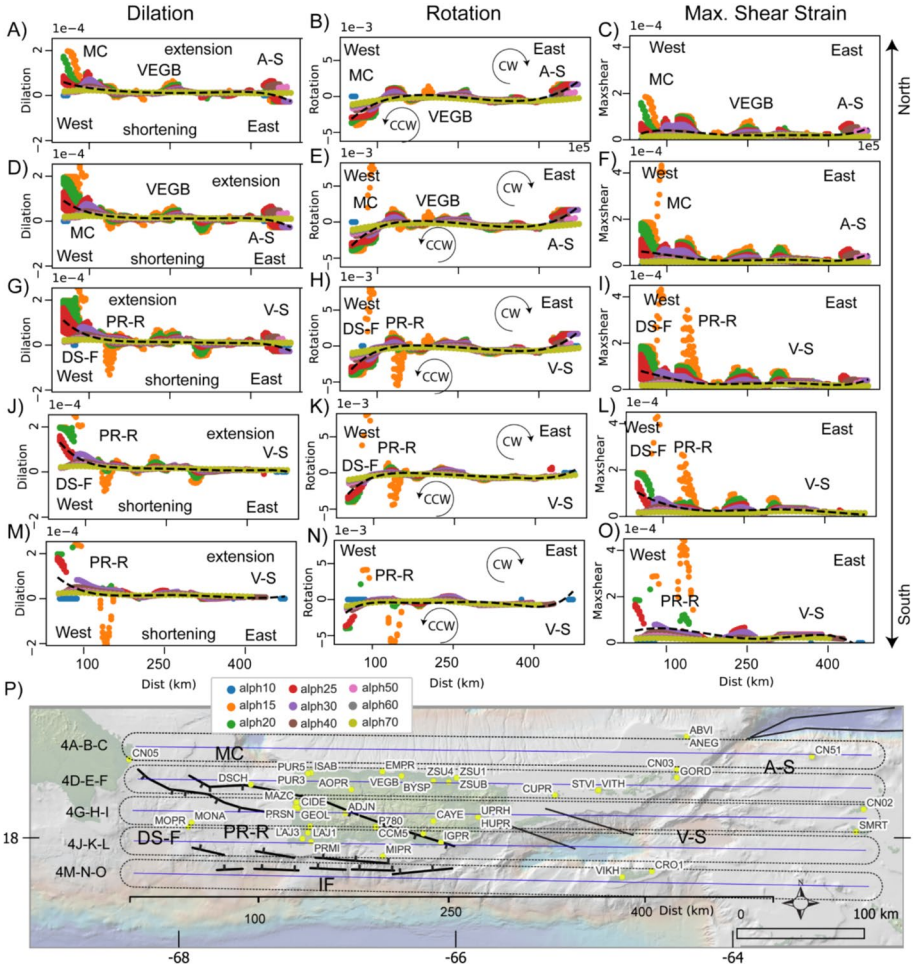

Fig. 4 **A** to **O** represents the crosssection of strain rates. Low alpha values ($\alpha = 15$, $\alpha = 35$) highlight interactions between nearby stations, demonstrating high but localized values suggesting strain accumulations in specific regions. In contrast, in high alpha values ($\alpha = 40$, $\alpha = 70$), the strain distribution across these graphs becomes notably smoother and less intense, suggesting a regional deformation. The dashed black line represents the best-fit line. **P** The map shows the cross-section in blue lines. Mc, Mona Canyon. DS-F, Desecheo Fault. PR-R, Puerto Rico rifting. V-S, Viequez segment. A-S, Anegada segment. VEGB is the GPS station locations. Yellow dots are GNSS stations

in local areas and on the regional scale (Fig. 4A–O). Significant positive dilation is also observed between 66°W and 65°W in the V-S and the region between 63°W and 63.5°W south of A-S (Fig. 5).

From Mona Canyon to PR-R (Fig. 4), positive dilation peaks at 2.5×10^{-4}, while negative dilation drops to -2×10^{-4} and indicates areas of contraction in the north and expansion in the south in the PR-R. From VEGB to PR-R section (Fig. 4), the dilation peaks reach up to 0.25×10^{-4} in the south, suggesting less intense but notable strain than other regions. From V-Sn to PR-R (Fig. 4), the dilation values range between -2.5×10^{-4} and 0.25×10^{-4}, showing a mix of contraction and extension strain. In contrast, zones of negative dilation between 67°W and 68.5W and at 65W suggest localized contraction areas. Positive dilation is prominent from 18.4 to 17°N, decreasing northward, primarily observable in low and medium alpha values, suggesting a more localized structure in southern Puerto Rico (Fig. 4).

Sections from Mona Canyon to A-S (Fig. 4) show positive dilation peaks around 1.5×10^{-4}. For PR-R, Lajas, east of GSPRF, and Vieques (Fig. 4), positive dilation reaches up to 2.5×10^{-4}. The map view (Fig. 5) shows spatial distribution with alpha = 25, as according to the alpha variability graphs, this value provides a good balance between local and regional structures and can represent dilation in Puerto Rico more appropriately. Between the stations MORP, MONA, DSCH, and CN05, an area with positive dilation extends from the west of Mona Canyon to the coast of Hispaniola, correlating with the western part of the Desecheo Fault. No significant data is available for the Mona Canyon. However, near the west coast of Puerto Rico, including stations south of Puerto Rico (MAZC, CIDE, DDJN, P780, CCM5, MIPR, PRMI, LAJ1, LAJ2, LAJ3, PRSN, Fig. 5), the greatest positive dilation or extension is found. This positive dilation coincides with the structural style observed in the fault patterns in the Mona Canyon, DS, GSPRF, and IF segments and in areas of high seismicity.

4.4.2 Rotation

Rotation detected with low alpha values ($\alpha = 15$, $\alpha = 30$) allows for detailed mapping of the rotational behavior in various parts of Puerto Rico. Significant clockwise (CW) rotation observed in the south and eastern regions near IF-E and V-S suggests localized rotational dynamics influenced by underlying geological structures within the PR-R (Fig. 5). This localized effect is contrasted by more widespread counterclockwise (CCW) rotation observed in northern areas like VEGB and North Vieques, which may indicate different subsurface conditions or strain distributions. High alpha values ($\alpha = 50$, $\alpha = 70$) provide smoother rotational patterns, indicating broader, less intense rotational dynamics. Changes in the trend line from negative to positive suggest shifts in rotational behavior, signifying underlying tectonic changes (Fig. 4).

From Mona Canyon to PR-R, rotation values range from -5×10^{-3} (CCW) to 4×10^{-4} (CW), indicating a significant range of rotational strain (Figs. 4 and 5). From VEGB to PR-R (Fig. 4), rotation peaks around -1×10^{-3} (CCW) to 1.5×10^{-3} (CW), suggesting areas of both counterclockwise and clockwise rotational strain. The rotation values in the North Vieques to PR-R (Fig. 4) range from -1×10^{-3} (CCW) to 1×10^{-4} (CW), which values suggest a less intense rotational strain in this area.

Longitudinal sections from Mona Canyon to A-S (Fig. 4) show rotation values ranging from -1×10^{-3} (CCW) to 1×10^{-3} (CW). For PR-R, east of GSPRF, and V-S (Fig. 4), rotation values range from -5×10^{-3} (CCW) to 2.5×10^{-3} (CW). These rotation patterns,

Fig. 5 The maps show the deformation pattern based on "alpha = 25 km". The distribution of deformation is visualized in two dimensions, showing variations along latitude and longitude in three different types of deformation: **A** Maximum shear, Principal infinitesimal horizontal strain axes white are extension and yellow are shortening. **B** Dilation, two-dimensional dilatation rate. Red is positive or extensional, and blue is negative. **C** Rotation, show the rotation about a vertical, downward positive axis, with red indicating clockwise (CW) and blue indicating counterclockwise (CCW)

alongside the MaxShear and dilation values, provide a comprehensive view of the strain behaviors across these regions. Rotation values further elucidate the strain distribution across the regions.

4.4.3 MaxShear (Maximum Shear Strain)

Maximum shear strain values are particularly concentrated in regions such as Mona Canyon (MC), VEGB, and the north Vieques segment along the north. This high value is particularly noticeable within the Puerto Rico rifting (PR-R), defined by the Desecheo (DS-F), Greater Puerto Rico Southern Fault (GSPRF), and Investigator faults, showing significant localized variations (Fig. 5).

Specifically, the Mona Canyon to Puerto Rico rifting (PR-R) shows values reaching up to 4×10^{-4} (Fig. 4), while from VEGB to PR-R (Fig. 4), there are high localized values at low alphas, with MaxShear peaking at 1.0×10^{-4}. Additionally, the north Vieques segments to PR-R show even higher peaks up to 8×10^{-4} (Fig. 4). These substantial peaks highlight local zones and suggest areas of intense shear strain, particularly at low alpha values. The longitudinal sections from Mona Canyon to, east of GSPRF and V-S (Fig. 4), also exhibit high shear strain peaks at low alpha values. Similar strain distribution patterns are observed for PR-R, east of GSPRF, and V-S, indicating that these regions experience significant shear strain (Fig. 4).

Conversely, increasing alpha values ($\alpha = 50$, $\alpha = 70$) makes the strain distribution across these graphs notably smoother and less intense, suggesting more uniform deformation across broader geographical regions. This pattern indicates that while extreme local strains are critical, the overall geological stability might be less perturbed across larger areas. However, specific sectors, such as those between south ZSU4-CAYE and east of GSPRF, continue to show a rising trend even at higher alpha values, hinting at potential regional deformation processes that might be less apparent at lower resolutions.

The best-fit dashed black line across these plots identifies the general/regional direction and magnitude of strain changes and alpha values, providing a visual summary that complements the detailed point data. In the map view, this strain distribution aligns with the geological structures, showing high shear strain zones, particularly to the south of the Desecheo Fault and between the Mona Canyon's eastern edge and the west of the Puerto Rico coast. These zones taper off towards the center of the island but increase again near Vieques.

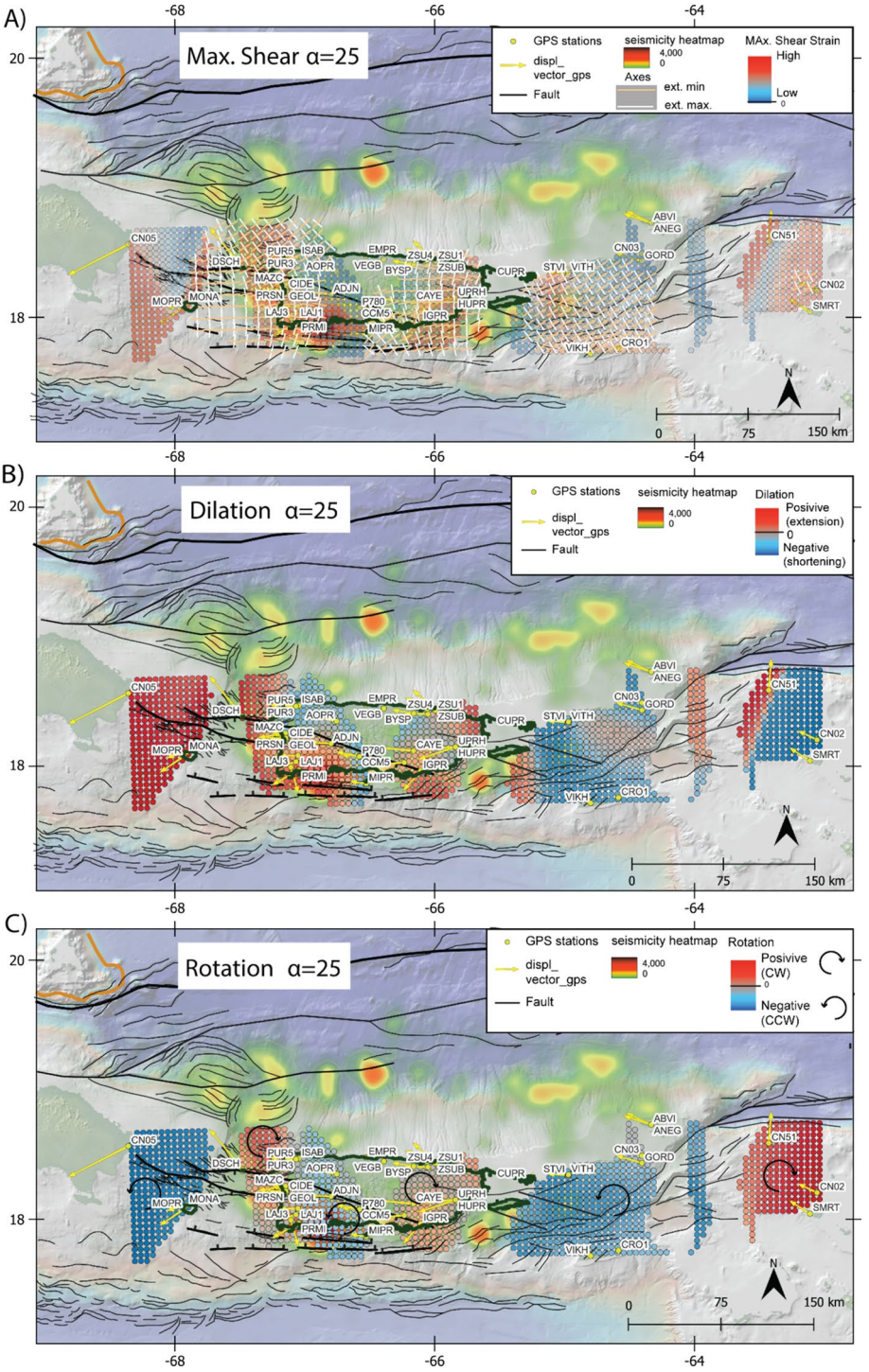
A)
Max. Shear α=25
GPS stations
displ_ vector_gps
Fault
seismicity heatmap
4,000
0
Axes
ext. min
ext. max.
MAx. Shear Strain
High
Low
B)
Dilation α=25
Dilation
Posivive (extension)
Negative (shortening)
C)
Rotation α=25
Rotation
Posivive (CW)
Negative (CCW)
-68
-66
-64
20
18
CN05
DSCH
PUR5
ISAB
PUR3
AOPR
MAZC
CIDE
PRSN
GEOL
MOPR
MONA
LAJ3
LAJ1
PRMI
EMPR
ZSU4
ZSU1
VEGB
BYSP
ZSUB
CUPR
ADJN
R780
CCM5
MIPR
CAYE
IGPR
UPRH
HUPR
STVI
VITH
VIKH
CRO1
ABVI
ANEG
CN03
GORD
CN51
CN02
SMRT
N
0
75
150 km

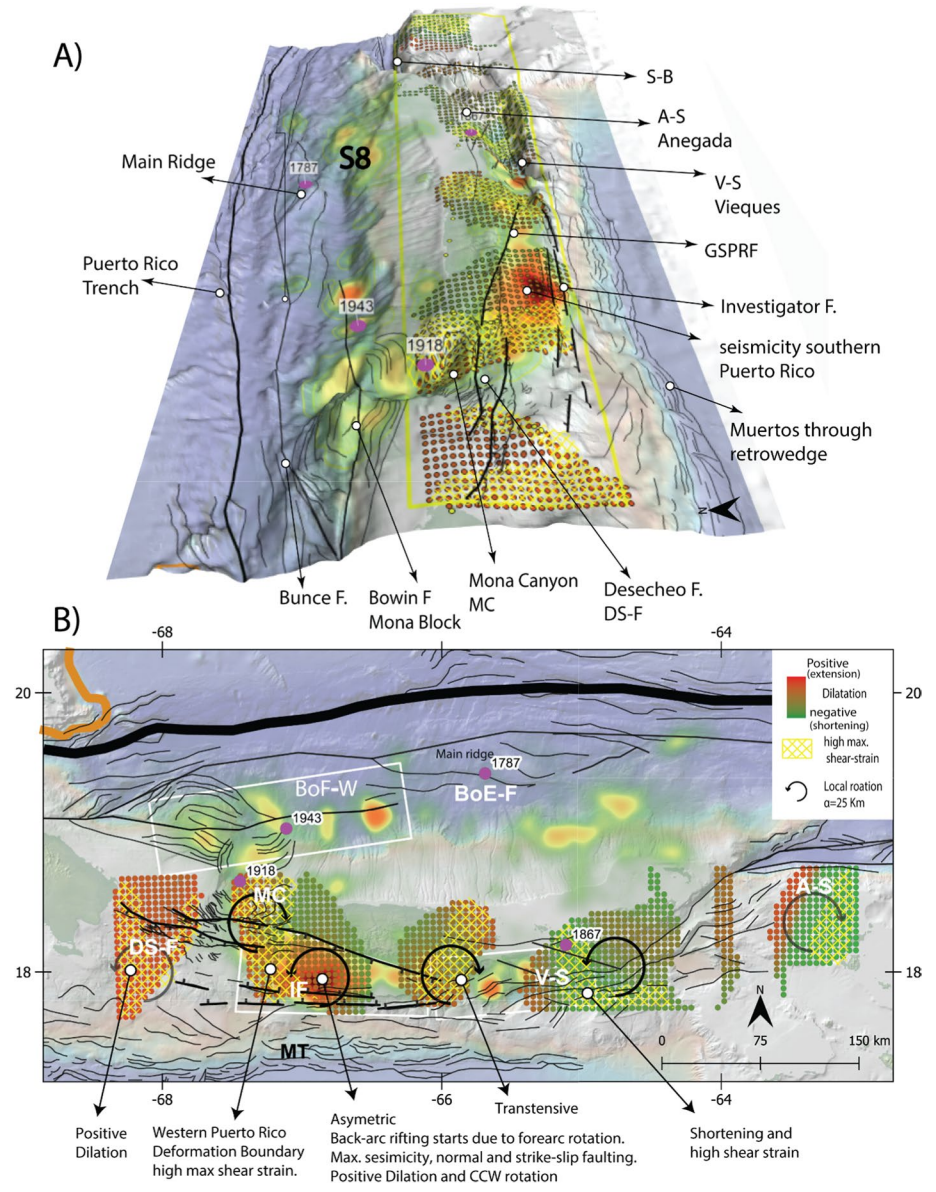

Fig. 6 The Tectonic model illustrates deformation transfer mechanisms from the trench to the Puerto Rico and Virgin Islands regions. The model highlights the fault patterns, seismicity, dilation, and maximum shear strain. White boxes are the areas with the higher tsunamigenic potential. PR-R, Puerto Rico rifting, includes IF, DS-F, and GSPRF segments. MC, Mona Canyon. BoF-W, Bowin Fault West. S8, seismic swarm described below. A-S, Anegada Segment. V-S, Vieques segment

5 Discussion

5.1 Current deformation distribution

Our model (Fig. 6) provides a detailed perspective on how deformation transfers from the subduction zone to the upper plate in the tectonic framework of Puerto Rico and the Virgin Islands. Dominant contractional forces, driven by the collision with the Bahamas Platform to the west, transfer stress to the upper plate. This process forms fold-thrust structures within the submarine accretionary wedge near Hispaniola (Dillon et al. 1992). Eastward, the tectonic regime transitions from the collision zone to a non-collided area characterized by a 25° counterclockwise rotation of Puerto Rico during the late Miocene-Pliocene. This rotation coincides with the arching of the Puerto Rico–Virgin Islands platform and normal faulting in the Mona Rift, driven by margin-perpendicular extension between Puerto Rico and Hispaniola (Reid et al. 1991; Gill et al., 1999; Mann et al., 2004, 2005).

The transition between collided and non-collided areas channels the deformation to the upper plate through the Western Puerto Rico Deformation Boundary (ten Brink et al., 2021). This boundary is particularly active in the north, extending from the BoF-W (Mona block) to Hispaniola. A rollover structure with normal displacement along a northeastern trend characterizes this region. Seismic activity and structural patterns indicate a negative flower structure, with NW–SE trending sub-vertical faults and subsiding blocks to the north. Grindlay et al. (2005) suggested this pattern could reflect the scar of a subducted seamount. However, it could also result from the sinistral motion of the Bowin Fault, which generates tensional fractures associated with a change in the strike direction of the main fault plane. These fractures are observed in the seismic lines of Mondziel et al. (2010), where they dip toward the main fault plane. This dipping geometry implies a direct mechanical relationship between the main fault and the secondary structures. The fractures likely represent zones of localized extension created by stress reorientation at the intersection of the Bowin Fault and the changing strike of the principal fault plane. Regardless of their genesis, notable seismic events have occurred in the region, including two large earthquakes approximately 510–720 and 2430–3220 years ago (Tuttle et al. 2023), suggesting ongoing deformation and indicating that these structures are not relics but remain active under the current tectonic regime.

The Western Puerto Rico Deformation Boundary separates Hispaniola from Puerto Rico but remains diffuse and poorly defined due to low deformation rates (ten Brink et al., 2021; Lopez-Venegas et al., 2023). Its diffuse nature suggests that amalgamating minor faults into one or a few major faults could necessitate significantly longer geological periods (Brink et al., 2021).

The dynamics within the Western Puerto Rico Deformation Boundary are influenced by fluctuations in seismic coupling along the Puerto Rico subduction interface, characterized by high coupling north of Hispaniola and the Mona Passage and minimal coupling north of Puerto Rico (Symithe et al., 2015; ten Brink et al., 2021). These fluctuations in seismic coupling imply that deformation along the Western Puerto Rico Deformation Boundary is most pronounced near the collision zone (Fig. 1) and diminishes with increasing distance, as demonstrated by ten Brink and Lin (2004). However, the significant concentration of seismic activity and the highest recorded values of infinitesimal deformation (dilation, extension) in the southern part of Puerto Rico, far from the Bahamas Platform collision and the Mona Canyon, may indicate minimal influence from this tectonic event (Fig. 6). Meanwhile, the fault pattern (Fig. 3A) suggests an abrupt termination of the Mona Canyon against the Desecheo Fault, indicating a lack of structural continuity between the forearc and backarc faults. Moreover, the extensive extensional and dilational deformation detected

by GPS in southern Puerto Rico does not manifest through continuous northward structures, suggesting localized deformation.

Our results indicate that the principal planes of maximum shear strain are confined to the Mona Canyon and the western coast of Puerto Rico (Fig. 6). In this context, the canyon acts as a structural depression situated between the geologically anchored Hispaniola and the dynamically mobile Puerto Rico and Virgin Islands. Despite the uncertain evidence of seismic activity along faults of southern Puerto Rico, seismic reflection lines consistently reveal growth strata with discernible vertical slips along the Desecheo and Investigator faults (Granja-Bruña et al., 2009; Chaytor and ten Brink, 2013). This data implies that these faults have been active concurrent with the collision of the Bahamas Platform with Hispaniola, suggesting favored development of structures since the Pliocene. Conversely, structures associated with the Western Puerto Rico Deformation Boundary of similar age remain diffuse and underdeveloped, likely corresponding to second-order structures observed in segments DS-F, GSPRF, IF-E, and IF-W. The Western Puerto Rico Deformation Boundary could correspond to a region of maximum shear strain (MaxShear) that traverses two significant structural domains: the Mona Canyon (MC) and the Puerto Rico rifting (PR-R) which include the Desecheo Fault and Investigator Fault. This boundary actively influences the secondary structural features within each structural domain (Fig. 6).

Therefore, it is highly probable that the Puerto Rico rifting is active and undergoing significant internal deformation, whereas the Muertos trench is currently inactive in its eastern sector. In this dynamic context, the Desecheo Fault and GSPRF to the north and the Investigator Fault to the south delineate the active Puerto Rico rifting. The rifting is characterized by slightly oblique normal slip second-order faults, such as the Lajas and Cerrillos faults, as observed in focal mechanisms near Guánica Bay (S11). The internal deformation in the Puerto Rico rifting is likely responsible for the intense seismic events such as the 2020 earthquake in Guánica Bay. This ongoing tectonic activity indicates a complex interplay of fault segments and rupture mechanisms, as suggested by various studies (Mann et al., 2002; Grindlay et al. 2005; Hippolyte et al. 2005; Jansma and Mattioli, 2005; ten Brink et al., 2021; Lopez-Venegas et al., 2023).

The GPS data reveals a substantial extension between the Investigator Fault and the GSPRF in the Puerto Rico backarc rifting. These rifting features exhibit transtensional characteristics where the fault zone boundaries are non-parallel and maintain a consistent slip vector, like the kinematic model proposed by Dewey (2002) for general transtensional systems. This geometric configuration results in an increased strain rate as the fault zone narrows, leading to vertical shortening and a consequent reduction in elevation.

We propose that the distribution of deformation to the upper plate can likely be attributed to the pivot generated in the BoF-W segment, where there is a change in the strike of the subduction zone, possibly associated with the collision of the Bahamas Platform, as Mann et al. (2005) and Wallace (2009) suggested. In this context, the Bahamas Platform, acting as a buoyant indentor, resists subduction beneath the Caribbean plate. The transition from subduction to collision leads to rapid fore-arc rotations (Fig. 6). This rapid rotation drives backarc rifting, where the backarc area begins to extend or split due to the tectonic forces exerted by the collision at the subduction zone. The presence of an indentor (such as the Bahamas Platform in the case of Puerto Rico) in the subduction system can significantly influence the rate of fore-arc rotation and the subsequent backarc rifting.

5.2 Tsunamigenic segments

The evaluation of tsunamigenic potential is based on four criteria: potential magnitude, fault length, historical activity, and current deformation. Faults capable of generating earthquakes ≥ Mw 8 or exceeding 250 km in length receive the highest scores. Intense historical seismicity and significant current deformation also score high, while segments with no recent activity are excluded.

Bowin Fault West (BoF-W) has a high tsunami potential, reflected in a total score of 9. This fault is characterized by its capacity to generate large-magnitude earthquakes due to its length. Historically, BoF-W has been active, with multiple significant seismic events recorded, and the current deformation in the region indicates continuous strain accumulation. Given its proximity to densely populated areas, there is a high risk of direct impact in the event of a seismic event. Bowin Fault East (BoF-E), with a total score of 7, shows considerable potential due to its expected magnitude and length. Although its historical activity and current deformation are moderate, the combination suggests significant, especially due to its location near populated areas. Bunce Fault (BuF-E, BuF-C, BuF-W), with scores of 7–6, although it has high potential magnitude and considerable length, shows low historical activity and current deformation, which reduces its total score but still suggests monitoring due to its structural capacity and location.

Investigator Fault (IF-N), scoring 7, stands out for its recent high activity and capacity to generate large earthquakes. Its extensive length and consistent deformation indicate significant strain accumulation. The Investigator Fault South segment (IF-S), with 6 points, although less active than its eastern counterpart, is still important due to its length and high current deformation, indicating strain accumulation. Vieques Segment (V-S) with a score of 6, exhibits moderate potential magnitude due to its combination of strike-slip and normal fault activities. Although its length is not as extensive as other major faults, it can produce significant earthquakes. The regular seismic activity, combined with modest current deformation, though not extremely intense, suggests less recent activity than more active areas. Mona Canyon (MC), with a score of 5, has a history of significant tsunamigenic earthquakes, highlighting its capacity to generate large vertical displacements of the seafloor, which is crucial for tsunami generation. Segments such as Desecheo Fault, SB and Muertos Thrugth show low historical activity and current deformation, with a score of 5. Finally, GSPRF has a lower score of 4.

Segment	Mw score	Length score	Activity score	Total score
BoF-W	3	3	3	9
BoF-E	3	3	1	7
BuF-C	3	3	1	7
BuF-W	3	3	1	7
IF-N	2	2	3	7
IF-S	1	2	3	6
BuF-E	2	3	1	6
V-S	2	1	3	6
SB-n	1	3	1	5
Sb-s	1	2	2	5
MC	2	1	2	5
DF-n	1	3	1	5

Segment	Mw score	Length score	Activity score	Total score
DF-s	1	3	1	5
MT	1	3	1	5
GSPRF	1	2	1	4

6 Conclusion

The Puerto Rico region is situated in a highly active tectonic setting, with a history of large-magnitude earthquakes and tsunami-generating events. Despite prior studies on tsunamigenic sources, the geometry, segmentation, and deformation dynamics of key fault systems remain poorly constrained. This gap in knowledge limits the accuracy of tsunami hazard assessments and inundation modeling.

To address these challenges, we compiled and analyzed an extensive dataset of seismic reflection lines, historical seismicity records, GNSS-derived strain measurements, and focal mechanism solutions. Faults were classified based on structural segmentation criteria, and their tsunamigenic potential was assessed using empirical magnitude-length relationships, historical earthquake occurrences, and current deformation rates.

The GNSS-derived strain analysis provided insights into the distribution of extensional and compressional strain across the region, identifying zones of active deformation that correlate with known fault structures. Strain analysis revealed that the highest deformation rates are concentrated in the Mona Canyon, Puerto Rico rifting zone (PR-R), and along the Western Puerto Rico Deformation Boundary. These regions exhibit significant extensional forces, indicating ongoing fault movement and potential for future seismic events.

The study identified several fault segments with significant tsunamigenic potential based on their capacity to generate large-magnitude earthquakes, historical seismic activity, and current strain accumulation. The Bowin Fault West (BoF-W) segment emerged as the most tsunamigenic fault, exhibiting a high potential for Mw 8 earthquakes and significant historical seismicity. Other high-risk segments include the Bowin Fault East (BoF-E), Bunce Fault segments (BuF-E, BuF-C, BuF-W), Investigator Fault (IF-N, IF-S), Vieques Segment (V-S), and Mona Canyon (MC), which have demonstrated considerable strain accumulation and seismic activity.

Funding This work was supported by the National Tsunami Hazard Mitigation Program (NTHMP), through the Puerto Rico component of the program, funded by the National Oceanic and Atmospheric Administration (NOAA). The project was implemented by the Puerto Rico Seismic Network (PRSN).

Declarations

Conflict of interest The authors declare that they have no conflict of interest.

References

Allmendinger RW, Reilinger R, Loveless J (2007) Strain and rotation rate from GPS in Tibet, Anatolia, and the Altiplano. Tectonics. https://doi.org/10.1029/2005TC001907

Allmendinger RW, Loveless JP, Pritchard ME, Meade B (2009) From decades to epochs: spanning the gap between geodesy and structural geology of active mountain belts. J Struct Geol 31(11):1409–1422. https://doi.org/10.1016/j.jsg.2009.10.011

Barkan R, Ten Brink U (2010) Tsunami simulations of the 1867 Virgin Island earthquake: constraints on epicenter location and fault parameters. Bull Seismol Soc Am 100(3):995–1009. https://doi.org/10.1785/0120090252

Blasweiler M, Herman MW, Houtsma F, Govers R (2022) Tectonic context and possible triggering of the 2019–2020 Puerto Rico earthquake sequence. Seismol Res Lett 93(2A):584–593. https://doi.org/10.1785/0220210217

Bouysse P, Westercamp D (1990) Subduction of Atlantic aseismic ridges and Late Cenozoic evolution of the Lesser Antilles island arc. Tectonophysics 175(4):349–380. https://doi.org/10.1016/0040-1951(90)90169-T

Calais É, Symithe S, Mercier de Lépinay B, Prépetit C (2016) Plate boundary segmentation in the northeastern Caribbean from geodetic measurements and Neogene geological observations. C R Geosci. https://doi.org/10.1016/j.crte.2015.10.007

Cardozo N, Allmendinger RW (2009) SSPX: a program to compute strain from displacement/velocity data. Comput Geosci 35(6):1343–1357. https://doi.org/10.1016/j.cageo.2008.05.007

Case JE, Holcombe TL, Martin PG (1984) Map of geologic provinces in the Caribbean region: Geological Society of America Memoir 162, p. 1–30.

Chaytor JD, ten Brink US (2010) Extension in Mona Passage, Northeast Caribbean. Tectonophysics. https://doi.org/10.1016/j.tecto.2010.07.002

Clifton AE, Schlische RW, Withjack MO, Ackermann RV (2000) Influence of rift obliquity on fault-population systematics: results of experimental clay models. J Struct Geol 22(10):1491–1509. https://doi.org/10.1016/S0191-8141(00)00043-2

DeMets C, Gordon RG, Argus DF (2010) Geologically current plate motions. Geophys J Int 181(1):1–80. https://doi.org/10.1111/j.1365-246X.2009.04491.x

Dewey JF, Holdsworth RE, Strachan RA (1998) Transpression and transtension zones. Geol Soc Lond Spec Publ 135(1):1–14. https://doi.org/10.1144/GSL.SP.1998.135.01.01

Dillon WP, Austin JA, Scanlon KM, Terence Edgar N, Parson LM (1992) Accretionary margin of northwestern Hispaniola: Morphology, structure, and development of part of the northern Caribbean plate boundary. Mar Pet Geol. https://doi.org/10.1016/0264-8172(92)90005-Y

Dolan JF, Wald DJ (1998) The 1943–1953 north-central Caribbean earthquakes: active tectonic setting, seismic hazards, and implications for Caribbean-North America plate motions. Geol Soc Am Spec Pap 326:143–169

Doser D, Rodríguez C, Flores C, Mann P (2005) Historical earthquakes of the Puerto Rico-Virgin Islands region. In: Mann P (ed) Active tectonic and seismic hazards of Puerto Rico, the Virgin Islands, and offshore areas. Geological Society of America, Boulder, pp 103–114. https://doi.org/10.1130/0-8137-2385-x.31

Gardner WD, Glover LK, Hollister CD (1980) Canyons off northwest Puerto Rico: studies of their origin and maintenance with the nuclear research submarine NR-1. Mar Geol 37(1–2):41–70. https://doi.org/10.1016/0025-3227(80)90010-3

Geist EL, ten Brink US (2021) Earthquake magnitude distributions on northern Caribbean faults from combinatorial optimization models. J Geophys Res Solid Earth 126(10):e2021JB022050

Gibbon S, Lorito S, de la Asunción M, Volpe M, Selva J, Macías J, Løvholt F (2022) The sensitivity of tsunami impact to earthquake source parameters and Manning friction in high-resolution inundation simulations. Front Earth Sci. https://doi.org/10.3389/feart.2022.642715

Granja Bruña JL, ten Brink US, Carbó-Gorosabel A, Muñoz-Martín A, Gómez Ballesteros M (2009) Morphotectonics of the central Muertos thrust belt and Muertos Trough (northeastern Caribbean). Mar Geol 263(1–4):7–33. https://doi.org/10.1016/j.margeo.2009.03.010

Granja Bruña JL, Muñoz-Martín A, ten Brink US, Carbó-Gorosabel A, Llanes Estrada P, Martín-Dávila J et al (2010) Gravity modeling of the Muertos Trough and tectonic implications (northeastern Caribbean). Mar Geophys Res. https://doi.org/10.1007/s11001-010-9107-8

Granja Bruña JL, Carbó Gorosabel A, Muñoz Martín A, Gómez Ballesteros M (2006) Cinturón Deformado de Los Muertos (Noreste de la Placa Caribe): Análisis Morfotectónico y Procesos Activos.

Grindlay NR, Mann P, Dolan JF, van Gestel JP (2005) Neotectonics and subsidence of the northern Puerto Rico-Virgin Islands margin in response to the oblique subduction of high-standing ridges. Geol Soc Am Spec Pap. https://doi.org/10.1130/0-8137-2385-x.31

Hippolyte JC, Mann P, Grindlay NR (2005) Geologic evidence for the prolongation of active normal faults of the Mona rift into northwestern Puerto Rico. Geol Soc Am Spec Pap 385:161–171. https://doi.org/10.1130/0-8137-2385-x.13

Huérfano V, von Hillebrandt-Andrade C, Báez-Sanchez G, Mann P (2005) Microseismic activity reveals two stress regimes in southwestern Puerto Rico. In: Mann P (ed) Active tectonics and seismic hazards of Puerto Rico, the Virgin Islands, and offshore areas. Geological Society of America Special Papers, Boulder, pp 81–101. https://doi.org/10.1130/0-8137-2385-x.8

Huérfano V (2003) Susceptibilidad de Puerto Rico ante el efecto de maremotos locales. PhD dissertation, Departamento de Ciencias Marinas, Universidad de Puerto Rico, Recinto de Mayagüez.

Jany I, Scanlon KM, Mauffret A (1990) Geological interpretation of combined Seabeam, Gloria and seismic data from Anegada Passage (Virgin Islands, north Caribbean). Mar Geophys Res 12:173–196. https://doi.org/10.1007/BF00369151

Lallemand SE, Schnürle P, Malavieille J (1994) Coulomb theory applied to accretionary and non accretionary wedges: possible causes for tectonic erosion and/or frontal accretion. J Geophys Res Solid Earth 99(B6):12033–12055. https://doi.org/10.1029/94JB00130

Laó-Dávila DA (2014) Collisional zones in Puerto Rico and the northern Caribbean. J S Am Earth Sci 54:1–19. https://doi.org/10.1016/j.jsames.2014.05.001

Larue DK (1994) Puerto Rico and the Virgin Islands. In: Donovan SK, Jackson TA (eds) Caribbean geology, an introduction. UWI Press, Kingston, pp 151–165

Laurencin M, Marcaillou B, Graindorge D, Klingelhoefer F, Lallemand S, Laigle M, Lebrun JF (2017) The polyphased tectonic evolution of the Anegada Passage in the northern Lesser Antilles subduction zone. Tectonics 36(5):945–961. https://doi.org/10.1002/2017TC004488

Laurencin M, Graindorge D, Klingelhoefer F, Marcaillou B, Evain M (2018) Influence of increasing convergence obliquity and shallow slab geometry onto tectonic deformation and seismogenic behavior along the Northern Lesser Antilles zone. Earth Planet Sci Lett 492:59–72. https://doi.org/10.1016/j.epsl.2018.03.052

Laurencin M, Marcaillou B, Graindorge D, Lebrun JF, Klingelhoefer F, Boucard M, Schenini L (2019) The Bunce fault and strain partitioning in the northern Lesser Antilles. Geophys Res Lett 46(16):9573–9582. https://doi.org/10.1029/2019GL083490

Mann P, Calais E, Huérfano V (2004) Earthquake shakes "Big Bend" Region of North America-Caribbean Boundary Zone. Eos Trans AGU 85(8):77–83. https://doi.org/10.1029/2004EO080001

Mann P, Prentice CS, Hippolyte JC, Grindlay NR, Abrams LJ, Laó-Dávila D (2005) Reconnaissance study of Late Quaternary faulting along Cerro Goden fault zone, western Puerto Rico. Geol Soc Am Spec Pap 385:115–138. https://doi.org/10.1130/0-8137-2385-x.11

Martinez A, Malavielle J, Lallemand S, Collot JY (2002) Partition de la déformation dans un prisme d'accrétion sédimentaire en convergence oblique: Approche expérimentale. Bull Soc Geol Fr 173(1):17–24. https://doi.org/10.2113/173.1.17

Masson DG, Scanlon KM (1991) The neotectonic setting of Puerto Rico. Geol Soc Am Bull 103(1):144–154. https://doi.org/10.1130/0016-7606(1991)103%3c0144:TNSOPR%3e2.3.CO;2

Matthews J, Holcombe T (1974) Possible Caribbean underthrusting of the Greater Antilles along the Muertos Trough. In: Transactions of the 7th Caribbean geological conference (Guadeloupe), pp 235–242.

McCalpin JP (2009) Application of paleoseismic data to seismic hazard assessment and neotectonic research. Int Geophys 95:1–106. https://doi.org/10.1016/S0074-6142(08)00001-4

McCann WR (1985) On the earthquake hazards of Puerto Rico and the Virgin Islands. Bull Seismol Soc Am 75:251–262

Meighan HE, Pulliam J, ten Brink U, López-Venegas AM (2013) Seismic evidence for a slab tear at the Puerto Rico Trench. J Geophys Res Solid Earth 118(6):2915–2923. https://doi.org/10.1002/jgrb.50215

Mercado A, McCann W (1998) Numerical simulation of the 1918 Puerto Rico tsunami. Nat Hazards 18:57–76. https://doi.org/10.1023/A:1007991420336

Mondziel S, Grindlay N, Mann P, Escalona A, Abrams L (2010) Morphology, structure, and tectonic evolution of the Mona canyon (northern Mona Passage) from multibeam bathymetry, sidescan sonar, and seismic reflection profiles. Tectonics. https://doi.org/10.1029/2008TC002441

Monroe WH (1980) Geology of the middle Tertiary formations of Puerto Rico. US Geol Surv Prof Pap 953.

Mueller C, Frankel A, Petersen M, Leyendecker E (2010) New seismic hazard maps for Puerto Rico and the US Virgin Islands. Earthq Spectra 26(1):169–185. https://doi.org/10.1193/1.3283178

Pindell JL, Draper G (1991) Stratigraphy and geological history of the Puerto Plata area, northern Dominican Republic. Spec Pap Geol Soc Am. https://doi.org/10.1130/SPE262-p97

Prentice CS, Mann P (2005) Paleoseismic study of the South Lajas fault: First documentation of an onshore Holocene fault in Puerto Rico. In: Mann P (ed) Active tectonics and seismic hazards of Puerto Rico,

the Virgin Islands, and offshore areas. Geological Society of America, Boulder, pp 215–222. https://doi.org/10.1130/0-8137-2385-x.15

Raussen S, Lykke-Andersen H, Kuijpers A (2013) Tectonics of the Virgin Islands Basin, northeastern Caribbean. Terra Nova 25(3):252–257. https://doi.org/10.1111/ter.12031

Reid JA, Plumley PW, Schellekens JH (1991) Paleomagnetic evidence for late Miocene counterclockwise rotation of north coast carbonate sequence, Puerto Rico. Geophys Res Lett 18(3):565–568. https://doi.org/10.1029/91GL00520

Rodríguez-Zurrunero A, Granja-Bruña JL, Carbó-Gorosabel A, Muñoz-Martín A, Gorosabel-Araus JM, Gómez de la Peña L et al (2019) Submarine morpho-structure and active processes along the North American-Caribbean plate boundary (Dominican Republic sector). Mar Geol. https://doi.org/10.1016/j.margeo.2018.10.010

Rodríguez-Zurrunero A, Granja-Bruña JL, Muñoz-Martín A, Leroy S, ten Brink U, Gorosabel-Araus JM et al (2020) Along-strike segmentation in the northern Caribbean plate boundary zone (Hispaniola sector): tectonic implications. Tectonophysics 776:228322. https://doi.org/10.1016/j.tecto.2020.228322

Román Y, Pujols E, Cavosie A, Stockli D (2020) Timing and magnitude of progressive exhumation and deformation associated with Eocene arc-continent collision in the NE Caribbean plate. Geol Soc Am Bull. https://doi.org/10.1130/B35715.1

Ryan WBF, Carbotte SM, Coplan J, O'Hara S, Melkonian A, Arko R et al (2009) Global multi-resolution topography (GMRT) synthesis data set. Geochem Geophys Geosyst 10(3):Q03014. https://doi.org/10.1029/2008GC002332

Schell B, Tarr A (1978) Plate tectonics of the northeastern Caribbean Sea Region. Geol Mijnbouw 57:139

Solares Colón MM (2019) New constraints on crustal deformation within the Puerto Rico-Virgin Islands microplate using two decades of GPS data [Thesis]. https://hdl.handle.net/20.500.11801/2492

Speed RC, Larue DK (1991) Extension and transtension in the plate boundary zone of the northeastern Caribbean. Geophys Res Lett 18(3):573–576. https://doi.org/10.1029/91GL00522

ten Brink U (2005) Vertical motions of the Puerto Rico Trench and Puerto Rico and their cause. J Geophys Res Solid Earth. https://doi.org/10.1029/2004JB003459

ten Brink U, Lin J (2004) Stress interaction between subduction earthquakes and forearc strike-slip faults: modeling and application to the northern Caribbean plate boundary. J Geophys Res Solid Earth. https://doi.org/10.1029/2004JB003031

ten Brink US, López-Venegas AM (2012) Plate interaction in the NE Caribbean subduction zone from continuous GPS observations. Geophys Res Lett. https://doi.org/10.1029/2012GL051485

ten Brink US, Bakun WH, Flores CH (2011) Historical perspective on seismic hazard to Hispaniola and the northeast Caribbean region. J Geophys Res Solid Earth. https://doi.org/10.1029/2011JB008497

ten Brink U, Wei Y, Fan W, Granja-Bruña J, Miller N (2020) Mysterious tsunami in the Caribbean Sea following the 2010 Haiti earthquake possibly generated by dynamically triggered early aftershocks. Earth Planet Sci Lett 540:116269. https://doi.org/10.1016/j.epsl.2020.116269

ten Brink US, Vanacore EA, Fielding EJ, Chaytor JD, López-Venegas AM, Baldwin WE et al (2022) Mature diffuse tectonic block boundary revealed by the 2020 southwestern Puerto Rico seismic sequence. Tectonics 41(3):e2021TC006896. https://doi.org/10.1029/2021TC006896

Thompson Jobe J, Briggs R, Hughes KS, Joyce J, Gold R, Mahan S et al (2024a) Neotectonic mapping of Puerto Rico. Seismica. https://doi.org/10.26443/seismica.v3i1.1102

Thompson Jobe J, Briggs RW, ten Brink U, Pratt TL, Hughes KS, Hatem AE et al (2024b) Geologic input databases for the 2025 Puerto Rico—US Virgin Islands National Seismic Hazard Model update: Crustal faults component. Seismol Res Lett. https://doi.org/10.1785/0220230222

Tuttle MP, et al (2023) Review of paleoliquefaction data, evaluation of scenario earthquakes, and estimation of source areas, magnitudes, and recurrence of large earthquakes impacting Puerto Rico and the US Virgin Islands. NEHRP Final Report G21AP10006. https://earthquake.usgs.gov/cfusion/external_grants/research.cfm

van Benthem S, Govers R, Spakman W, Wortel R (2013) Tectonic evolution and mantle structure of the Caribbean. J Geophys Res Solid Earth 118(6):3019–3036. https://doi.org/10.1002/jgrb.50235

van Gestel JP, Mann P, Dolan JF, Grindlay NR (1998) Structure and tectonics of the upper Cenozoic Puerto Rico-Virgin Islands carbonate platform as determined from seismic reflection studies. J Geophys Res Solid Earth 103(B12):30505–30530. https://doi.org/10.1029/98JB02203

Vogt PR, Lowrie A, Bracey DR, Hey RN (1976) Subduction of aseismic oceanic ridges: Effects on shape, seismicity, and other characteristics of consuming plate boundaries. Geological Society of America, Boulder

Wallace LM, Ellis S, Mann P (2009) Collisional model for rapid fore-arc block rotations, arc curvature, and episodic back-arc rifting in subduction settings. Geochem Geophys Geosyst. https://doi.org/10.1029/2008GC002220

Authors and Affiliations

Hernán Porras[1,2] · Víctor Huérfano[2] · José Mescua[3,4] · Alberto López-Venegas[2]

✉ Hernán Porras
hernan.porras@upr.edu

Víctor Huérfano
victor.huerfano@upr.edu

José Mescua
jmescua@mendozaconicet.gob.ar

Alberto López-Venegas
alberto.lopez3@upr.edu

[1] Department of Marine Sciences, University of Puerto Rico, UPRM-Campus, Mayaguez, PR 00680, USA

[2] Puerto Rico Seismic Network, Department of Geology, University of Puerto Rico, UPRM-Campus, Mayagüez, PR 00680, USA

[3] Instituto Argentino de Nivología, Glaciología y Ciencias Ambientales (IANIGLA), CCT Mendoza, CONICET, Parque General San Martín, 5500 Mendoza, Argentina

[4] Facultad de Ciencias Exactas y Naturales, Universidad Nacional de Cuyo, Padre Jorge Contreras 130, Parque General San Martín, 5502 Mendoza, Argentina